Static fluxons in a superlattice of Josephson junctions

2002 J. Phys. A: Math. Gen. 35 10409

(http://iopscience.iop.org/0305-4470/35/48/313)

INSTITUTE OF PHYSICS PUBLISHING JOURNAL OF PHYSICS A: MATHEMATICAL AND GENERAL

J. Phys. A: Math. Gen. **35** (2002) 10409–10427 PII: S0305-4470(02)53202-9

Static fluxons in a superlattice of Josephson junctions

Y Gaididei[1,2], N Lazarides[2] and N Flytzanis[2]

[1] Institute for Theoretical Physics, 252143 Kiev, Ukraine
[2] Physics Department, University of Crete, 71409 Heraklion, Greece

Received 12 September 2002
Published 19 November 2002
Online at stacks.iop.org/JPhysA/35/10409

Abstract
A planar superlattice of Josephson junctions is studied theoretically and numerically. The superlattice is made of laterally coupled long Josephson tunnel junctions through idle regions. Static fluxon solutions are found analytically and numerically. For narrow junctions the problem is reduced to a system which is effectively nonlocal in space. We explore the nonlocality effects on the local magnetic field components, the Josephson current and the energy density, for a coherent homopolar fluxon array.

PACS number: 74.50.+r

1. Introduction

There has been a great interest in the last few years in the study of long Josephson junctions as a means for the generation of rf waves in the gigahertz region. They can compete with semiconductor based rf oscillators in the region above 100 GHz due to low noise, power and size. It is well known by now that a long Josephson junction is a nonlinear device which supports self-resonant solitonic modes (fluxons). A bias current applied to the junction causes fluxons to move along the junction. As soon as the fluxon reaches the junction end it radiates an electromagnetic pulse, and it is reflected back. Thus in this type of oscillator, a fluxon moves between the junction ends, emitting radiation whenever it reaches the boundary. The frequency f of the radiation is determined by the junction length L and the fluxon velocity u, and is given by $f = u/2L$. The linewidth of the radiation is determined by the fluctuations of the fluxon velocity.

In general, one is interested in increasing the output power of the radiation and making its linewidth narrower. It has been found that phase-locking of N fluxon oscillators indeed increases the output power as N^2, and makes the linewidth narrower. This is the reason why phase-locked arrays of fluxon oscillators are of technological interest today. Phase-locking is achieved through coupling of fluxons in different oscillators. Thus, in the last few years various types of phase-locked oscillators have been studied, such as parallel arrays of small Josephson junctions either one-dimensional [1], or two-dimensional [2, 3], vertically stacked

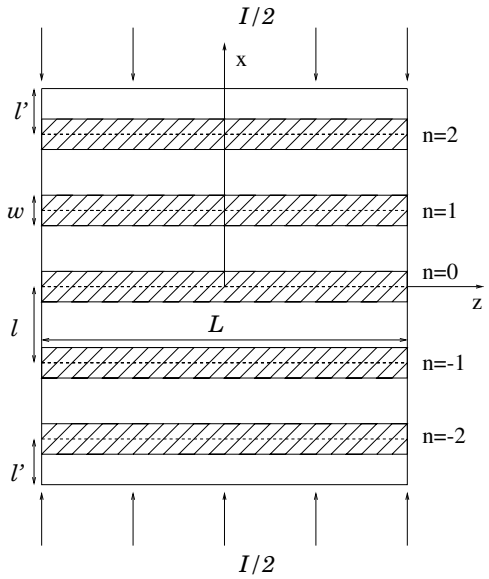

Figure 1. Schematic planar view of a Josephson junction superlattice.

long Josephson junctions [4–6], and laterally coupled long Josephson junctions [7, 8]. In many cases the experimentalists managed to achieve phase-locking.

We shall consider the problem of N laterally coupled long Josephson junctions, which are coupled through idle (or passive) regions, where there is no Josephson current. In other words, we have an alternating structure of passive and active waveguides. This structure is advantageous, because the idle regions cause a considerable increase of the fluxon limiting velocity, thus increasing the frequency of the emitted radiation. The other advantage is that the lateral idle region introduces dispersion [9] and therefore we have the possibility of wave emission due to the Cherenkov phenomenon. The frequency of this radiation depends on the value of the driving current and can be continuously varied.

In the following section, we shall describe the model and derive the nonlocal equations for the phase differences of the junctions. According to the method employed, the Laplace problems in the idle regions are solved, and subsequently they are coupled to the equations in the junctions through the boundary conditions at the interfaces. This method is common in the theory of antennas [10]. In section 3, we give the analytical static solution of coherent fluxon motion along all junctions, together with the numerical solution. The results are valid for all widths of the idle region, but we also give the solutions for the extreme cases of very small and very large nonlocality, i.e. small or large idle region. In section 4, we give the theoretical formulae for the magnetic field components, the Josephson current and the energy density. Finally, in the last section we discuss the results and present the conclusions.

2. Superlattice model and equations of motion

We consider a two-dimensional Josephson junction which consists of two superconducting metal plates (parallel to the x–z plane) separated by a thin oxide layer of variable thickness (figure 1). The electromagnetic behaviour of such a system is governed by Maxwell's equations

coupled with the Josephson current–phase relation

$$J_y(x,z,t) = J(x)\sin\phi(x,z,t) \tag{1}$$

for the tunnelling supercurrent density through the oxide layer, and the Josephson voltage–phase relation

$$V(x,z) = \frac{\hbar}{2e}\partial_t\phi(x,z,t). \tag{2}$$

In equations (1) and (2) $\phi(x,z,t)$ is the phase difference of the order parameters between the two superconductors and ∂_t is the partial time derivative. The maximum Josephson current density J depends on the material properties and on the thickness d of the oxide layer. We will consider an alternating structure and assume that the thickness $d(x)$ is a periodic function of the space coordinate x of the form

$$d(x) = \begin{cases} d_j & \text{if} \quad |x-\ell n| < \frac{w}{2} \quad n = 0, \pm1, \pm2, \dots \\ d_i & \text{otherwise} \end{cases}$$

where w is the width of the window and ℓ ($\ell \geqslant w$) is the width of the idle region. Thus the centres of the junctions are separated by $\Delta x = \ell$. We consider a contrasting periodic structure with $d_i \gg d_j$, so that due to the sharp exponential dependence of the Josephson current on the thickness of the isolating layer $d(x)$ we can assume that there is no Josephson current in the regions with thick oxide layer d_i:

$$J(x) = \begin{cases} J_c & \text{if} \quad |x-\ell n| < \frac{w}{2} \quad n = 0, \pm1, \pm2, \dots \\ 0 & \text{otherwise.} \end{cases}$$

In this way the system under consideration is a periodic structure of Josephson junctions (windows) separated by the idle regions.

If the thickness $d(x)$ of the oxide layer is small compared with the London penetration depths λ_1, λ_2 of the two superconducting films, a two-dimensional approach to this problem is quite satisfactory [11] and the electrodynamics of the system is governed by the (2 + 1)-dimensional sine-Gordon type equation with x-dependent parameters,

$$\left(\partial_x^2 + \partial_z^2\right)\phi = \frac{1}{c^2(x)}\partial_t^2\phi + \frac{1}{\Lambda_j^2(x)}\sin\phi \tag{3}$$

where the quantity

$$c(x) = c_0\sqrt{\frac{d(x)}{\epsilon(\lambda_1+\lambda_2)}}$$

is the local velocity of electromagnetic waves, ∂_x denotes the spatial derivative with respect to x, etc, ϵ is the dielectric constant of the oxide layer, μ_0 the permeability of vacuum, c_0 is the speed of light in vacuum and $\Lambda_j(x)$ is the local Josephson penetration length equal to

$$\lambda_j = \sqrt{\frac{h}{2eJ_c\mu_0(\lambda_1+\lambda_2)}}$$

in the windows, while it tends to infinity in the idle regions.

Assuming that the width of the window w is small compared with the Josephson penetration length, that is $w \ll \lambda_j$, we can regard the phase ϕ to be independent of the coordinate x inside the window layer. In this case we can shrink the junction to a delta function but scale up the critical current by a factor of w, so that the integrated critical current

through each junction remains the same. Then the Josephson current given by equation (1), can be written as

$$J_y(x,z,t) = w\sum_n j_n(z,t)\delta(x-x_n) \tag{4}$$

with

$$j_n = \frac{1}{\lambda_j^2}\sin\phi(x_n,z,t) \tag{5}$$

where j_n is the current through a single window junction. As is shown in appendix A, the problem of the superlattice with very narrow junctions (as in equation (3) with equation (4)) can be presented in the form

$$\left(\partial_x^2+\partial_z^2-g(x)\partial_t^2\right)\phi = f(x)\frac{1}{\lambda_j^2}\sin\phi \tag{6}$$

where

$$g(x) = \frac{1}{v_i^2}+\frac{1}{v_j^2}f(x) \tag{7}$$

with the structure function

$$f(x) = w\sum_n \delta(x-x_n) \tag{8}$$

where $x_n = n\ell, n = 0, \pm1, \pm2, \ldots,$ and

$$v_i^2 = \frac{d_i c_0^2}{\epsilon(\lambda_1+\lambda_2)} \qquad v_j^2 = \frac{d_j c_0^2}{\epsilon(\lambda_1+\lambda_2)} \tag{9}$$

are the phase velocities in idle regions and windows, respectively.

The numerical solution of equation (6) in the space domain of the superlattice requires extensive calculations, which are not necessary because in most of the domain (except at $x = n\ell, n = 0, \pm1, \pm2, \ldots$) the system obeys linear equations. These equations can be solved in the striped idle regions and connected to the solution in the narrow junctions. This will lead to a system of coupled partial differential equations for the phase on the junctions $\phi_n(z,t) \equiv \phi(x = n\ell, z, t)$. Thus the nonlinearity is along one-dimensional domains.

Using the Fourier transform with respect to z and t

$$\bar\phi(x,k,\omega) = \frac{1}{(2\pi)^2}\int_{-\infty}^{\infty}\mathrm{d}z\int_{-\infty}^{\infty}\mathrm{d}t\,\phi(x,z,t)\,\mathrm{e}^{-\mathrm{i}(kz-\omega t)} \tag{10}$$

where the bars distinguish the Fourier transformed quantities, one can represent equations (6)–(8) in the form

$$-\kappa^2\bar\phi(x,k,\omega)+\partial_x^2\bar\phi(x,k,\omega) = w\sum_n\delta(x-x_n)\left[\frac{1}{\lambda_J^2}\overline{\sin\phi}(x,k,\omega)-\frac{\omega^2}{v_j^2}\bar\phi(x,k,\omega)\right] \tag{11}$$

where the left-hand side vanishes outside the junction lines, and

$$\kappa = \sqrt{k^2-\frac{\omega^2}{v_i^2}}. \tag{12}$$

In equation (11) the system obeys

$$-\kappa^2\bar\phi(x,k,\omega)+\partial_x^2\bar\phi(x,k,\omega) = 0$$

everywhere except at $x = x_n = n\ell$. In each domain $n\ell < x < (n+1)\ell$ the solution can be written as

$$\bar{\phi}(x, k, \omega) = A_n \, \mathrm{e}^{-\kappa x} + B_n \, \mathrm{e}^{\kappa x}$$

where the coefficients A_n, B_n can be written through the boundary conditions at $x = n\ell$ and $x = (n+1)\ell$ as functions of the phases $\phi_n(z, t)$ and $\phi_{n+1}(z, t)$. Across the nth junction due to the delta functions we have discontinuities in the derivatives of ϕ. These derivatives involve the constants A_n, B_n, and the corresponding ones A_{n-1}, B_{n-1} in the domain below, which can be eliminated by the boundary conditions for $\phi(x, z, t)$ at $x = n\ell - 0$ and $x = (n-1)\ell + 0$, i.e. the edges of the $(n-1)$th idle region. The boundary conditions of the discontinuity of the derivatives at $x = n\ell$ will give us a sine-Gordon type equation for ϕ_n coupled to the phases ϕ_{n+1} and ϕ_{n-1}.

Thus, eliminating the waves in the linear media following the procedure used in appendix A and applying the inverse Fourier transformation with respect to equation (10), leads to the following expression for the field $\phi(x, z, t)$ for $\ell \gg w$ in terms of the phases at the nonlinear layers: $\phi_n(z, t) \equiv \phi(x_n, z, t)$

$$\phi(x, z, t) = -\frac{\sinh[\hat{\kappa}(x - (n+1)\ell)]}{\sinh(\hat{\kappa}\ell)}\phi_n(z, t) + \frac{\sinh[\hat{\kappa}(x - n\ell)]}{\sinh(\hat{\kappa}\ell)}\phi_{n+1}(z, t) \tag{13}$$

for $n\ell \leqslant x \leqslant (n+1)\ell$ with $n = 0, \pm 1, \pm 2, \ldots$, where the phases $\phi_n(z, t)$ can be found from the set of coupled equations

$$\frac{\hat{\kappa}}{\sinh \ell\hat{\kappa}}(\phi_{n+1} + \phi_{n-1}) - 2\frac{\hat{\kappa}}{\tanh \ell\hat{\kappa}}\phi_n - \frac{w}{v_j^2}\partial_t^2\phi_n - \frac{w}{\lambda_j^2}\sin\phi_n = 0. \tag{14}$$

In equations (13) and (14) the operator $\hat{\kappa}$ is the Fourier multiplier operator defined by

$$\overline{\hat{\kappa}\phi}(k, \omega) \equiv \frac{1}{(2\pi)^2}\int_{-\infty}^{\infty} \mathrm{d}z \int_{-\infty}^{\infty} \mathrm{d}t \, \mathrm{e}^{-\mathrm{i}(kz - \omega t)} \sqrt{-\partial_z^2 + \frac{1}{v_i^2}\partial_t^2}\phi(z, t) = \sqrt{k^2 - \frac{\omega^2}{v_i^2}}\,\overline{\phi}(k, \omega). \tag{15}$$

Thus, the dynamics of the system is described by the set of pseudo-differential or, in other words, by nonlocal in time and space equations, taking into account the retarded behaviour demanded by causality. The nonlocal character of the window junction dynamics is due to the existence of two pathways for the energy transfer: directly along the window junction and through the idle regions. This is seen more clearly in appendix B.

The system of equations (14) is still very complicated. Further simplification can be achieved by taking into account that in contrast alternating structures ($d_i \gg d_j$) that we are interested in, the velocity of the electromagnetic waves is much higher in the idle region due to the decreased capacitance, that is $v_i \gg v_j$. Therefore, restricting ourselves to the investigation of low-frequency behaviour $\left(\frac{\omega\ell}{v_i} \ll 1\right)$, we shall neglect the effects of retarded time and consider the limit $v_i \to \infty$. In this limit equations (13) and (14) reduce to

$$\phi(x, z, t) = -\frac{\sinh[\hat{k}(x - (n+1)\ell)]}{\sinh(\hat{k}\ell)}\phi_n(z, t) + \frac{\sinh(\hat{k}(x - n\ell))}{\sinh(\hat{k}\ell)}\phi_{n+1}(z, t) \tag{16}$$

for $n\ell \leqslant x \leqslant (n+1)\ell$ ($n = 0, \pm 1, \pm 2, \ldots$), and the phase at the nth junction satisfies the equation

$$\frac{\hat{k}}{\sinh \ell\hat{k}}(\phi_{n+1} + \phi_{n-1}) - 2\frac{\hat{k}}{\tanh \ell\hat{k}}\phi_n - \frac{w}{c_j^2}\partial_t^2\phi_n - \frac{w}{\lambda_j^2}\sin\phi_n = 0 \tag{17}$$

where

$$\hat{k} = \sqrt{-\partial_z^2}.$$

The last equation can also be written in the integral form

$$\frac{2}{\pi}\int_{-\infty}^{\infty} d\zeta \ln\left[\coth\left(\frac{\pi}{2\ell}|\zeta - z|\right)\right]\partial_\zeta^2\phi_n(\zeta,t) + \frac{\pi}{4\ell^2}\int_{-\infty}^{\infty} d\zeta \operatorname{sech}^2\left[\frac{\pi}{2\ell}(\zeta - z)\right][\phi_{n+1}(\zeta,t) + \phi_{n-1}(\zeta,t) - 2\phi_n(\zeta,t)] - \frac{w}{\lambda_j^2}\sin\phi_n(z,t) - \frac{w}{v_j^2}\partial_t^2\phi_n(z,t) = 0. \tag{18}$$

From equation (18) we clearly see the nonlocal character of the junctions, so that we can describe the behaviour from the local limit, where there are only low order derivatives to the extreme nonlocal case where we obtain an integral equation.

In the extreme case of large ℓ ($\ell \to \infty$) there should be little coupling between junctions. This can be seen because the second term is proportional to $1/\ell^2$, and for the case where there are fluxons closely spaced in each junction (i.e. slightly displaced in each junction from the vertical), it can be disregarded. This is the extreme nonlocal limit, where the kernel reduces to that of Benjamin–Ono or sine-Hilbert [12].

It is also seen from equation (6) that the momentum

$$P = -\int_{-\infty}^{\infty} dx \int_{-\infty}^{\infty} dz\, g(x)\partial_t\phi\partial_z\phi \tag{19}$$

and the Hamiltonian

$$H = \int_{-\infty}^{\infty} dx \int_{-\infty}^{\infty} dz \left[g(x)\frac{1}{2}(\partial_t\phi)^2 + \frac{1}{2}(\partial_x\phi)^2 + \frac{1}{2}(\partial_z\phi)^2 + f(x)(1 - \cos\phi)\right] \tag{20}$$

are the integrals of motion, in the absence of damping, under the condition of periodic boundary conditions or vanishing derivatives at $z \to \pm\infty$ and $x \to \pm\infty$. These relations will be useful in the study of fluxons using the collective coordinate approach.

3. Static Josephson vortices

The solution is greatly simplified if we look at the time-independent problem. This means that we neglect capacitive effects by observing at low velocities of fluxon motion, or in the extreme case of static fluxons. As in the single window junction we expect that we still have fluxons whose width, however, is influenced strongly by the size of the idle region. It is natural, therefore, to see if we can obtain analytic solutions for a static coherent line of fluxons in an infinite length. This is interesting since if this coherent configuration can also be propagated we can have strong radiative effects.

For the static problem the phase ϕ does not depend on time. In this case the phases in the windows ϕ_n can be found from the set of equations

$$\frac{\hat{k}}{\sinh(\hat{k}\ell)}(\phi_{n+1} + \phi_{n-1}) - \frac{2\hat{k}}{\tanh(\hat{k}\ell)}\phi_n - \frac{w}{\lambda_j^2}\sin\phi_n = 0 \tag{21}$$

or the equivalent form

$$\frac{\hat{k}}{\sinh(\hat{k}\ell)}(\phi_{n+1} + \phi_{n-1} - 2\phi_n) - 2\hat{k}\tanh\left(\frac{\ell\hat{k}}{2}\right)\phi_n - \frac{w}{\lambda_j^2}\sin\phi_n = 0. \tag{22}$$

Introducing equation (13) into equation (20) we obtain that in the static case the energy of the system can be expressed in terms of the phase of window junctions $\phi_n(z)$ as follows:

$$H = \sum_n \int_{-\infty}^{\infty} dz \left[(\partial_z\phi_n)\frac{\tanh\left(\frac{\hat{k}\ell}{2}\right)}{\hat{k}}(\partial_z\phi_n) + (\phi_{n+1} - \phi_n)\frac{\hat{k}}{2\sinh(\hat{k}\ell)}(\phi_{n+1} - \phi_n)\right] + \sum_n \int_{-\infty}^{\infty} dz \frac{w}{\lambda_j^2}(1 - \cos\phi_n) \tag{23}$$

or equivalently

$$H = \sum_n \int_{-\infty}^{\infty} \mathrm{d}z \int_{-\infty}^{\infty} \mathrm{d}\zeta \left\{ \frac{1}{\pi} (\partial_z \phi_n) \ln \left[\coth \left(\frac{\pi}{2\ell} |\zeta - z| \right) \right] (\partial_\zeta \phi_n) \right.$$
$$\left. + \frac{\pi}{8\ell^2} [\phi_n(z) - \phi_{n+1}(z)] \operatorname{sech}^2 \left[\frac{\pi}{2\ell} (\zeta - z) \right] [\phi_n(\zeta) - \phi_{n+1}(\zeta)] \right\}$$
$$+ \frac{w}{\lambda_j^2} \sum_n \int_{-\infty}^{\infty} \mathrm{d}z [1 - \cos \phi_n(z)]. \tag{24}$$

One of the physically reasonable excitation patterns mentioned above is the configuration where the phases $\phi_n(z)$ are the same in all windows, i.e.

$$\phi_n(z) = \Phi(z). \tag{25}$$

For this excitation pattern the function $\Phi(z)$ satisfies the equation

$$\sqrt{-\partial_z^2} \tanh \frac{\ell \sqrt{-\partial_z^2}}{2} \Phi + \frac{w}{2\lambda_j^2} \sin \Phi = 0 \tag{26}$$

since the junction coupling terms cancel. In equation (26) we also wrote the explicit form of the operator $\hat{k}$. Using the dimensionless variable

$$\xi = \frac{w}{2\lambda_j^2} z \tag{27}$$

equation (26) can be written in the form

$$\sqrt{-\partial_\xi^2} \tanh \left(\frac{\nu}{4} \sqrt{-\partial_\xi^2} \right) \Phi + \sin \Phi = 0 \tag{28}$$

or equivalently using the definition (15) in the integral form

$$\frac{1}{\pi} \int_{-\infty}^{\infty} \mathrm{d}\xi' \ln \left[\coth \left(\frac{\pi}{\nu} |\xi - \xi'| \right) \right] \partial_{\xi'}^2 \Phi(\xi') - \sin \Phi(\xi) = 0 \tag{29}$$

where the nonlocality parameter

$$\nu = \frac{w\ell}{\lambda_j^2} \tag{30}$$

characterizes the significance of nonlocality effects in the system.

When $\nu \ll 1$, while at the same time $\ell > w$, and from equations (26) and (29) we obtain the usual pendulum equation

$$\frac{\nu}{4} \partial_\xi^2 \Phi - \sin \Phi = 0 \tag{31}$$

which has the well-known sine-Gordon fluxon solutions of the form

$$\Phi = 4 \arctan \left(\exp \left(\frac{2\lambda_j \xi}{\sqrt{w\ell}} \right) \right) \equiv 4 \arctan \left(\exp \left(\frac{z}{w_f} \right) \right). \tag{32}$$

where

$$w_f = \sqrt{\frac{\ell}{w}} \lambda_j \tag{33}$$

is the width of the fluxon.

When the distance ℓ between junctions becomes very large ($\nu \to \infty$), equation (31) takes the form

$$\mathcal{H}\{\partial_\xi \Phi\} - \sin \Phi = 0 \tag{34}$$

where the notation $\mathcal{H}\{f(x)\}$ stands for the Hilbert transform of $f(x)$, which is defined as

$$\mathcal{H}\{f(x)\} \equiv \mathcal{P}\frac{1}{\pi}\int_{-\infty}^{\infty} \mathrm{d}x' \frac{f(x')}{x'-x} \tag{35}$$

where $\mathcal{P}$ denotes the Cauchy principal value of the corresponding integral. This means that equation (26) reduces to the nonlinear sine-Hilbert equation whose solutions have the form of algebraic solitons [12]:

$$\Phi = \pi + 2\arctan(\xi) \equiv \pi + 2\arctan\left(\frac{wz}{2\lambda_J^2}\right). \tag{36}$$

Note that the same equation as equation (26) describes magnetic vortices in a distributed Josephson junction with electrodes of finite thickness [13]. An exact solution which corresponds to an isolated Josephson fluxon was found in [13]. We describe the derivation of this solution in more detail. We look for the solution of equation (26) which should yield for $\Phi(z)$ the result given by equation (31) in the limit $\nu \to 0$ whereas for $\ell \to \infty$ we expect to obtain $\Phi(z)$ in the form of equation (36). We seek the solution of equation (26) in the form

$$\Phi = 4\ \arctan(a\sinh(bz) + \sqrt{a^2\sinh^2(bz)+1}) \tag{37}$$

where a and b are parameters to be determined. In order to determine a, b we shall follow Joseph's approach in his search for solitary waves in a finite depth fluid [14]. Using the Fourier transform, equation (26) can be written as follows:

$$\tanh\left(\frac{k\ell}{2}\right) = \frac{w}{2\lambda_j^2}\frac{\overline{\sin\Phi}}{\overline{\mathrm{i}\partial_z\Phi}}. \tag{38}$$

Substituting equation (37) into equation (38), we obtain that equation (38) is satisfied if

$$a = \sec(\beta/2) \qquad b = \frac{\beta}{\ell} \tag{39}$$

where the new parameter β is defined in the interval $\beta \in (0, \pi)$ and is directly related to the physical parameters of the system by the following transcendental equation:

$$\beta\tan(\beta/2) = \frac{w\ell}{2\lambda_j^2} \equiv \frac{\nu}{2}. \tag{40}$$

Thus, the solution of equation (26) has the form

$$\Phi = 4\arctan\left[\sec\left(\frac{\beta}{2}\right)\sinh\left(\frac{\beta}{\ell}z\right) + \sqrt{\sec^2\left(\frac{\beta}{2}\right)\sinh^2\left(\frac{\beta}{\ell}z\right)+1}\right] \tag{41}$$

which can also be written as

$$\Phi = -2\arctan\left(\frac{\cos\frac{\beta}{2}}{\sinh\frac{\beta}{\ell}z}\right). \tag{42}$$

It is seen that when $\nu \to 0$ we have $\beta \to 0$ and we obtain from equation (40)

$$\frac{\beta}{\ell} \simeq \sqrt{\frac{w}{\lambda_j^2\ell}} \tag{43}$$

so that equation (41) reduces to the fluxon solution given by equation (32). When the distance between windows increases ($\ell \to \infty$), then

$$\beta = \pi(1-\epsilon) \qquad \text{with} \quad \epsilon \simeq \frac{4\lambda_j^2}{w\ell} \ll 1. \tag{44}$$

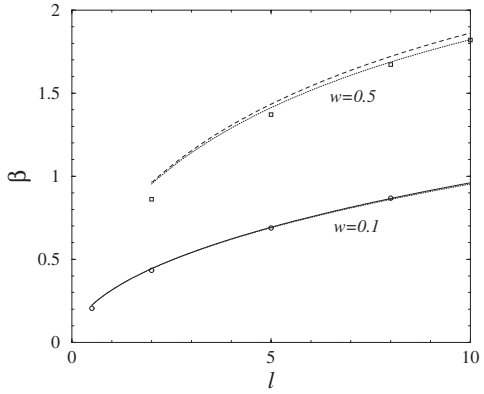

Figure 2. The exact solution for the parameter β for $w = 0.1$ (solid line) and $w = 0.5$ (dashed line) versus ℓ. The dotted lines are calculated from the interpolation formula for the same w. The points are numerical solutions including the extra local term.

In this case we obtain an algebraic soliton (equation (36))

$$\Phi = 4 \arctan\left(\frac{wz}{2\lambda_j^2} + \sqrt{\left(\frac{wz}{2\lambda_j^2}\right)^2 + 1}\right) \tag{45}$$

which is an equivalent form of equation (36) (see e.g. [12]).

Note that with a rather good accuracy the lhs of equation (40) in the interval $\beta \in (0, \pi)$ can be approximated as

$$\beta \tan(\beta/2) \simeq \frac{\pi^2}{2} \frac{\beta^2}{\pi^2 - \beta^2}. \tag{46}$$

Thus, from equations (40) and (46) one can obtain an interpolation formula for the parameter β:

$$\beta = \frac{\pi}{\sqrt{1 + \frac{\pi^2 \lambda_j^2}{w\ell}}} \tag{47}$$

which is a good approximation in the whole interval $[0, \pi]$ and it is exact in the two limits. In figure 2 we compare β versus ℓ from equation (40) (exact solution) and equation (47) (interpolation formula) for two values of w. From this figure we see that the interpolation formula agrees very well with the exact solution for β. We also give the parameter β from the direct numerical solution including the small local term proportional to w which was neglected. It was obtained by fitting the numerical results by the function $\Phi(z)$ given in equation (41) with β as the fitting parameter. We see that for $w = 0.1$ the agreement is very good and even for $w = 0.5$ the agreement is within 5% for $\ell > 4$.

Equation (26) can be solved numerically in the Fourier space for the Fourier components of the phase $\Phi(z)$. Thus, taking the Fourier transform of equation (26) we get

$$2k \tanh\left(\frac{k\ell}{2}\right) \bar{\Phi}_k + w\overline{[\sin\Phi(z)]}_k = 0 \tag{48}$$

where k takes the values $k_m = \frac{2\pi m}{L}$, with $m = 0, \pm 1, \pm 2, \ldots, \pm n_z$, and $n_z = 1024$ is the number of Fourier components. The system of equations is solved with a simple relaxation iteration scheme. For a relatively long junction, the numerical and the analytic solutions agree

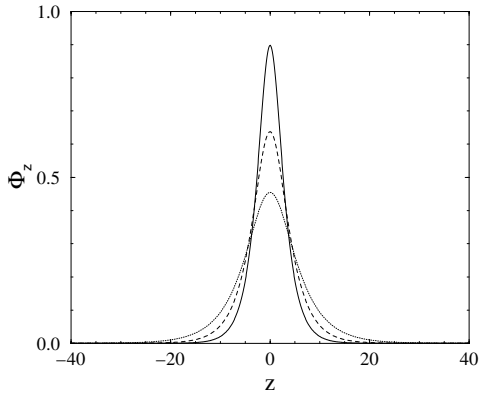

Figure 3. The fluxon profile Φ_z for $\ell = 0.5$ (solid line), $\ell = 1.0$ (dashed line) and $\ell = 2.0$ (dotted line). The other parameters are $w = 0.1$, $L = 80$.

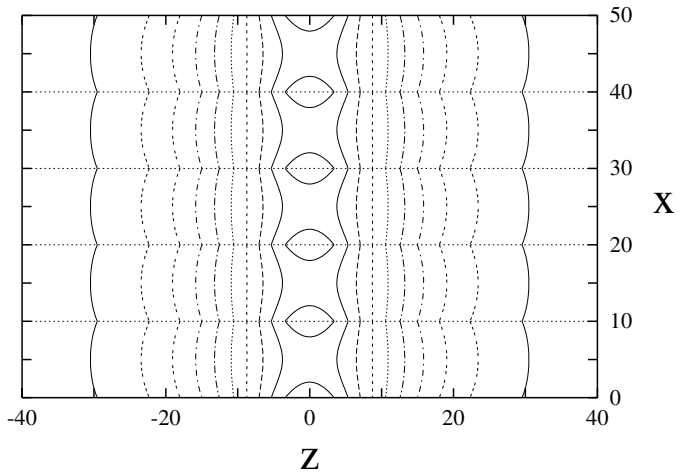

Figure 4. Contours of $\phi_z(x, z)$ in steps of 0.02 for $w = 0.1$, $\ell = 10.0$, $L = 80$. The horizontal dotted lines show the centre positions of the windows.

perfectly. For a short junction, there are differences close to the endpoints of the junction, due to boundary effects.

Some fluxon profiles for $L = 80$, $w = 0.1$, are shown in figure 3, for $\ell = 0.5$ (solid line), $\ell = 1.0$ (dashed line) and $\ell = 2.0$ (dotted line). One can see that the width of the fluxon profile decreases considerably with increasing ℓ. In the general case the parameter ℓ/β is a measure of the fluxon width. Here we remark that for the static problem the local $w\phi_{zz}$ term, which would add a term $wk^2\bar{\Phi}_k$ to the left-hand side of equation (48), can be neglected safely if $w \ll \ell$ and the fluxon width is large, which limits the range of significant k values.

In figure 4, we show the contours of $\phi_z(x, z)$ for $L = 80$, $w = 0.1$ and $\ell = 10.0$, for a superlattice with five windows. The horizontal dotted lines show the centre positions of the windows.

4. Energy density, fluxon content, Josephson current and magnetic field

The relation between the effective magnetic field $\vec{\mathcal{H}}$ and the phase difference ϕ is given by

$$\vec{\mathcal{H}} = -\hat{e}_y \times \vec{\nabla}\phi \tag{49}$$

where $\mathcal{H}$ is normalized to $\frac{2\pi\Phi_0}{\mu_0(\lambda_1+\lambda_2)\lambda_j}$, and $\hat{e}_y$ is the unit vector normal to the junction plane. It is seen that the magnetic pattern is two dimensional, so that it is necessary to define flux penetration along both directions. Thus according to equation (49) the effective magnetic field $\mathcal{H}$ is a two-dimensional vector in the plane of the barrier

$$\vec{\mathcal{H}} = (-\partial_z\phi, 0, \partial_x\phi). \tag{50}$$

The magnetic fluxes in units of the quantum flux $\Phi_0 = \frac{h}{2e}$ that penetrate the junction along the two directions are [15]

$$N_x = \frac{1}{2\pi}\int_{-\infty}^{\infty} \mathrm{d}z\, \mathcal{H}_x = \frac{1}{2\pi}(\phi(x,\infty) - \phi(x,-\infty)) \tag{51}$$

$$N_z = \frac{1}{2\pi}\int_{n\ell}^{(n+1)\ell} \mathrm{d}x\, \mathcal{H}_z = \frac{1}{2\pi}\,(\phi_n(z) - \phi_{n+1}(z)) \tag{52}$$

for $n\ell \leqslant x \leqslant (n+1)\ell$ with $n = 0, \pm1, \pm2, \ldots$. Note that the fluxon content N_x is a function of x while N_z is a function of z.

Combining equations (4), (16), (50), (25) and (41) one can obtain that the Josephson current through a single window $j_n(z) = j(z)$ and the components of the effective magnetic field $\vec{\mathcal{H}}$ can be written as follows:

$$j_n(z) = -\frac{2}{\lambda_j^2}\frac{\cos\left(\frac{\beta}{2}\right)\sinh\left(\frac{\beta}{\ell}z\right)}{\cos^2\left(\frac{\beta}{2}\right) + \sinh^2\left(\frac{\beta}{\ell}z\right)} \tag{53}$$

$$\mathcal{H}_x(x,z) = -4\frac{\beta}{\ell}\frac{\cos\left(\beta\left(n+\frac{1}{2}-\frac{x}{\ell}\right)\right)\cosh\left(\frac{\beta z}{\ell}\right)}{\cos\left(2\beta\left(n+\frac{1}{2}-\frac{x}{\ell}\right)\right) + \cosh\left(2\frac{\beta z}{\ell}\right)} \tag{54}$$

$$\mathcal{H}_z(x,z) = -4\frac{\beta}{\ell}\frac{\sin\left(\beta\left(n+\frac{1}{2}-\frac{x}{\ell}\right)\right)\sinh\left(\frac{\beta z}{\ell}\right)}{\cos\left(2\beta\left(n+\frac{1}{2}-\frac{x}{\ell}\right)\right) + \cosh\left(2\frac{\beta z}{\ell}\right)} \tag{55}$$

for $n\ell \leqslant x \leqslant (n+1)\ell$ with $n = 0, \pm1, \pm2, \ldots$. Expressions (54) and (55) give the magnetic field everywhere and are valid also in the windows from the continuity conditions used.

By an integration by parts in equation (29) and making use of the current conservation equation

$$J_y \equiv w\sin\phi_n = \partial_z J_{\mathrm{surf}} \tag{56}$$

we can define a local surface current $J_{\mathrm{surf}}(z)$ which is a nonlocal function of the phase gradient and is given as

$$J_{\mathrm{surf}}(z) = -\mathrm{i}\partial_z \tanh\frac{\ell\sqrt{-\partial_z^2}}{2}\Phi \equiv \int \mathrm{d}z'\, G(z-z')\partial_{z'}\phi_n(z') \tag{57}$$

where the kernel is given by

$$G(z-z') = \frac{\ell}{2\pi}\ln\left\{\tanh\frac{\pi}{\ell}|z-z'|\right\}. \tag{58}$$

For the coherent fluxon line considered, the surface current is given by

$$J_{\mathrm{surf}}(z) = \frac{w}{\lambda_j^2\tan\left(\frac{\beta}{2}\right)}\ln\frac{\cosh\left(\frac{\beta z}{\ell}\right) + \sin\left(\frac{\beta}{2}\right)}{\cosh\left(\frac{\beta z}{\ell}\right) - \sin\left(\frac{\beta}{2}\right)}. \tag{59}$$

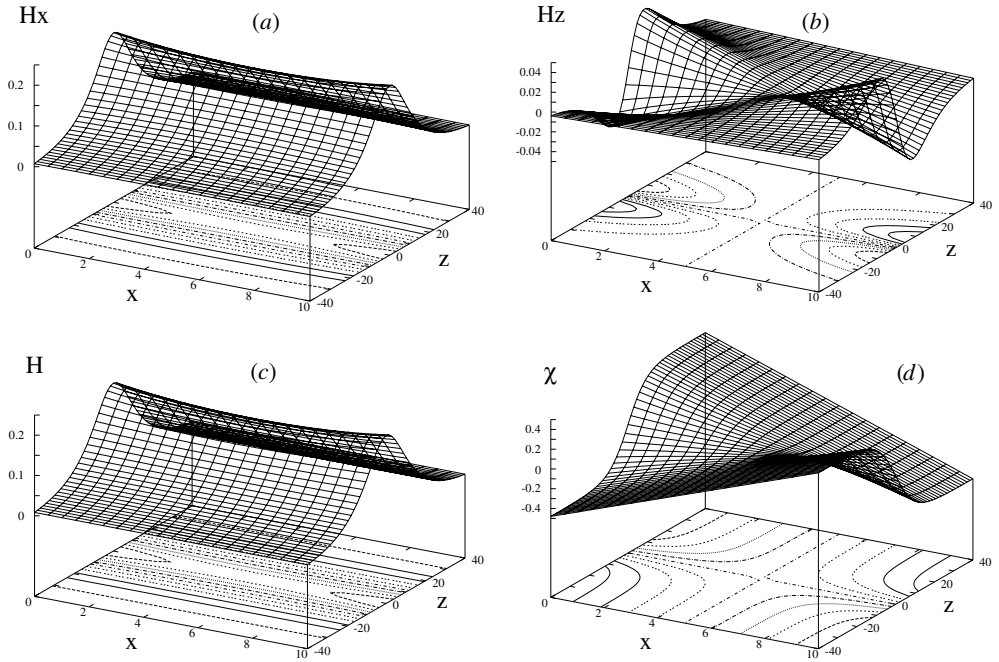

Figure 5. (*a*) The effective magnetic field component H_x, (*b*) the effective magnetic field component H_z, (*c*) the magnitude of $\vec{\mathcal{H}}$ and (*d*) the angle of the magnetic field $\chi = \tan^{-1}(H_x/H_z)$, all shown from the centre of the $n = 0$ window to the centre of the $n = 1$ window, for $L = 80$, $w = 0.1$, $\ell = 10$.

In the local limit $v \to 0$ it reduces to the sine-Gordon result $\frac{2w}{\lambda_j^2}\mathrm{sech}(z/w_f)$ equal to the local phase gradient. For deviations from the local limit for small v, the amplitude of the surface current is

$$A_s = 2w\left(1 + \tfrac{1}{24}v\right). \tag{60}$$

For larger ℓ the surface current deviates from $w\partial_z\Phi$.

Equations (54) and (55) show that while the normal component of the magnetic field $\mathcal{H}_x$ (the component which is perpendicular to the windows) is a symmetric function in both variables x and z, the tangential component $\mathcal{H}_z$ has a dipole-like behaviour: it changes sign at the centre of the fluxon ($z = 0$) and at the centre of the idle region $\left(x = \frac{\ell}{2}\right)$. In other words, one can say that the magnetic field rotates in the space between windows while at the same time it moves along the windows. The planar magnetic field components normal and parallel to the junction edge are shown in figures 5(*a*) and (*b*), respectively. In figures 5(*c*) and (*d*), we also show the magnitude of the magnetic field $\mathcal{H}$, and the phase χ, with $\chi = \tan^{-1}(H_x/H_z)$, respectively. χ is the angle of the magnetic field $\vec{\mathcal{H}}$ from the x-axis (positive direction). Thus at $z = 0$ the magnetic field is parallel to the x-axis. The same is true along the line $x = \ell/2$ for any z. If we see along the lower idle region edge, as we go away from $z = 0$ towards $z \to \pm\frac{L}{2}$ the angle χ approaches about $\pm 30^\circ$ correspondingly and the opposite signs hold along the upper boundary of the idle region. If we are at $z = -\frac{L}{2}$ and move up inside the idle region the direction of the magnetic field rotates from $\chi = -30^\circ$ to $+30^\circ$ and the opposite is true at the other end $z = +\frac{L}{2}$. This is consistent with the fact that in the idle region, due to the absence of Josephson energy, the magnetic lines tend to open up more near the centre of the idle region along $x = \ell/2$. In figure 6(*a*) we

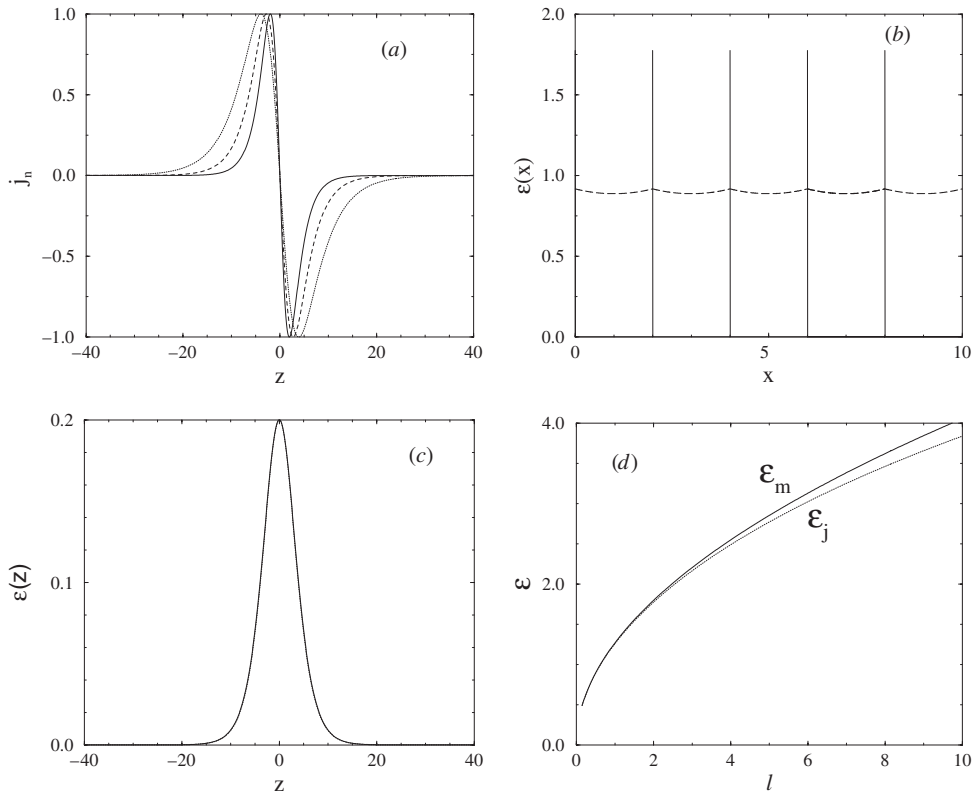

Figure 6. (*a*) The Josephson current through a single window, $J_n(z)$, for $\ell = 0.5$ (solid line), $\ell = 1.0$ (dashed line) and $\ell = 2.0$ (dotted line). The other parameters are $w = 0.1$, $L = 80$. (*b*) The energy density per unit width of the idle region, $\mathcal{E}(x)$, for $w = 0.1$, $\ell = 2.0$, $L = 80$, shown as two separate contributions: the magnetic energy density $\mathcal{E}_m$ (dashed line), and the Josephson energy density, $\mathcal{E}_j$ (solid line). (*c*) The energy density per unit length of the window, $\mathcal{E}(z)$, shown as two separate contributions: the magnetic energy density $\mathcal{E}_m$ (solid line) and the Josephson energy density, $\mathcal{E}_j$ (dashed line), for $w = 0.1$, $\ell = 2.0$, $L = 80$. (*d*) The integrated magnetic and Josephson energies versus the idle region width, ℓ ($w = 0.1$, $L = 80$).

plot the Josephson current through a single window, $j_n(z)$ for $L = 80$, $w = 0.1$ and $\ell = 0.5$ (solid line) $\ell = 1.0$ (dashed line) and $\ell = 2.0$ (dotted line). We see that with increasing ℓ the extrema in $j_n(z)$ shift. As we move along the tails to large z we still have an exponential behaviour at the junction ends. Thus we have two different scales for the width and only in the extreme case $\ell \to \infty$ do we have only one scale in the form of the algebraic fluxons.

When the nonlocality parameter is small ($\nu \ll 1$) we obtain from equations (53), (54) and (55)

$$\begin{aligned} j(z) &= -\frac{2}{\lambda_j^2}\frac{\sinh\left(\sqrt{\frac{w}{\lambda_j^2\ell}}z\right)}{\cosh^2\left(\sqrt{\frac{w}{\lambda_j^2\ell}}z\right)} \\ \mathcal{H}_x &\simeq -2\sqrt{\frac{w}{\lambda_j^2\ell}}\,\mathrm{sech}\left(\sqrt{\frac{w}{\lambda_j^2\ell}}z\right) \\ \mathcal{H}_z &\to 0. \end{aligned} \tag{61}$$

We see that in this case nonlocality effects are small and the behaviour of the phase difference, the current density and the magnetic field is the same as in a single Josephson junction [11].

When the distance between windows increases ($\ell \to \infty$) we get along the window

$$j(z) \simeq -\frac{2}{\lambda_j^2}\frac{\frac{zw}{\lambda_j^2}}{1+\left(\frac{zw}{\lambda_j^2}\right)^2} \qquad \mathcal{H}_x \simeq -\frac{w}{\lambda_j^2}\frac{1}{1+\left(\frac{zw}{\lambda_j^2}\right)^2} \qquad \mathcal{H}_z \simeq -\frac{w}{\lambda_j^2}\frac{\frac{zw}{\lambda_j^2}}{1+\left(\frac{zw}{\lambda_j^2}\right)^2}$$

where we used equation (44) and a Taylor expansion which is valid for $z < \frac{\ell}{\pi}$. Note that in contrast to the case of narrow idle regions, the nonlocal effects here change drastically the behaviour of the phase difference, the current density and the magnetic field: instead of the exponential law given by equations (61), now they decay algebraically $\left(\sim\frac{1}{|z|}\right)$ at the junction edges. For a finite length junction with $L \ll \frac{\ell}{\pi}$ the magnetic field is almost parallel to the junction away from $z = 0$ and the junction ends. In fact the ratio of the magnetic field at the idle region centre to that on the window for $z = 0$ and large ℓ is

$$\left|\frac{\mathcal{H}\left(x=\left(n+\frac{1}{2}\right)\ell, z=0\right)}{\mathcal{H}(x=n\ell, z=0)}\right| \to \frac{2}{\pi}\frac{\lambda_j^2}{w\ell}$$

and for $\ell \to \infty$ it goes to zero, i.e. the magnetic field lines are pushed towards the edges of the idle region. If the junction length $L \gg \frac{\ell}{\pi}$ then for $\ell \to \infty$ inside the idle region over the length $\frac{\ell}{\pi}$ the magnetic lines are pushed towards the ends, while outside this range the magnitude of $\mathcal{H}$ does not vary along x and the direction of $\mathcal{H}$ becomes almost vertical within $\Delta x \simeq 0.15\ell$.

It is interesting to see how the energy of the system varies along the normal to the window junctions. This behaviour is characterized by the following energy density per unit length of the x-axis:

$$\mathcal{E}(x) = \int_{-\infty}^{\infty} \mathrm{d}z \left[\frac{1}{2}(\partial_x\phi)^2 + \frac{1}{2}(\partial_z\phi)^2 + \frac{1}{\lambda_j^2}f(x)(1-\cos\phi)\right]. \tag{62}$$

Inserting equations (25) and (41) into equation (62) we obtain that the energy density per unit length of the idle region can be expressed as the sum

$$\mathcal{E}(x) = \mathcal{E}_m(x) + \mathcal{E}_j(x) \tag{63}$$

where

$$\mathcal{E}_m(x) = \frac{8\beta^2}{\ell^2}\sum_n \frac{\left(n+\frac{1}{2}\right)\ell - x}{\sin\frac{2\beta}{\ell}\left(\left(n+\frac{1}{2}\right)\ell - x\right)}(\theta(x-n\ell) - \theta(x-(n+1)\ell)) \tag{64}$$

is the density of magnetic energy of the system, and

$$\mathcal{E}_j(x) = 4\beta\sum_n \delta(x-n\ell) \tag{65}$$

is the energy density of the Josephson current. The magnetic energy density $\mathcal{E}_m(x)$ and the Josephson energy density $\mathcal{E}_j(x)$ are shown in figure 6(b), as dashed and solid lines, respectively, for $L = 80$, $w = 0.1$ and $\ell = 2.0$. The Josephson energy is stored only in the window region so it corresponds to the spikes while the magnetic energy is extended over the whole surface, and for the choice of parameters it is almost constant along x except for a small variation. The ratio between the minimum and the maximum values of the magnetic energy density is approximately 0.97. For finite ℓ, part of the magnetic energy is concentrated in the idle region:

$$\frac{\mathcal{E}_m\left(x=\left(n+\frac{1}{2}\right)\ell\right)}{\mathcal{E}_m(x=n\ell)} = \frac{\sin\beta}{\beta}. \tag{66}$$

This part depends on the physical parameters of the system through β. Recall that the Josephson part of the energy includes a delta function so that the integrated magnetic and Josephson energies are not very different (see figure 6(d) for comparison). In the limit of $\nu \to 0$ when the nonlocality effects are unimportant the magnetic energy contribution coincides with the Josephson one.

We can also see the variation of the energy density in the direction along the windows. We can write as before $\mathcal{E}(z)$ as a sum of the corresponding magnetic energy density and Josephson energy density $\mathcal{E}(z) = \mathcal{E}_m(z) + \mathcal{E}_j(z)$, where

$$\mathcal{E}_m(z) = \frac{1}{2}\int_{-\infty}^{+\infty} [(\partial_x\phi)^2 + (\partial_z\phi)^2]\,\mathrm{d}x \qquad \mathcal{E}_j(z) = Nw[1 - \cos\,\Phi(z)]$$

with N being the number of windows in the superlattice. The energy densities $\mathcal{E}_m$, $\mathcal{E}_j$, per unit length of the window are shown in figure 6(c), for $L = 80$, $w = 0.1$ and $\ell = 2.0$, as solid and dotted lines, respectively.

Finally, in figure 6(d) we plot the integrated magnetic and Josephson energies versus the idle region width, ℓ. Thus we see that in the local limit the Josephson energy is equal to the magnetic energy, while with increasing ℓ the magnetic energy increases faster. $\mathcal{E}_j$ increases with ℓ because the fluxon becomes wider. This should have the tendency to lower the magnetic energy in the window but is increased due to the enlarged width of the idle region. Asymptotically it becomes independent of ℓ. Note that for $\ell = 1$ the ratio $\frac{\mathcal{E}_m}{\mathcal{E}_j} \simeq 1.01$.

The Josephson energy per junction is for any ℓ equal to $\varepsilon_j = 4\beta$, which in the small ν and large ℓ limits correspondingly goes as

$$\mathcal{E}_j \simeq 4\beta \qquad \text{small } \nu \tag{67}$$

$$\mathcal{E}_j \simeq 4\pi\left(1 - \frac{4\lambda_j^2}{w\ell}\right) \qquad \text{large } \ell\ (\ell \to \infty) \tag{68}$$

i.e. approaches a constant value 4π like $1/\ell$.

From equation (64) the magnetic energy per junction, after some simple change of variables, is

$$E_m = 2\int_{-\beta}^{\beta} \mathrm{d}x \frac{x}{\sin x}. \tag{69}$$

The small ν limit can be written as a Taylor expansion keeping the first two terms

$$E_m \simeq 4\beta + \frac{2}{9}\beta^3 \tag{70}$$

while for large ℓ we have the logarithmic singularity of the two-dimensional problem, like

$$E_m \simeq -4\pi \ln\frac{\lambda_j^2}{w\ell} + c_\infty \tag{71}$$

where the constant c_∞ is independent of ℓ. From equation (69) the slope can be obtained as

$$\frac{\mathrm{d}E_m}{\mathrm{d}\ell} = 4\frac{\beta}{\sin\beta}\frac{\mathrm{d}\beta}{\mathrm{d}\ell} \tag{72}$$

with $\frac{\mathrm{d}\beta}{\mathrm{d}\ell}$ obtained from the slope of figure 2 or from the empirical relation (47). So in the limit of small ν we can estimate the slope at $\ell = 1$ to be nearly equal to 0.63, where we used $\frac{\mathrm{d}\beta}{\mathrm{d}\ell}(\ell = 1) \simeq 0.315$. This is very close to the slope in figure 6(d). The ratio of the slopes of E_m and E_j for any ℓ is

$$R \equiv \frac{\mathrm{d}E_m/\mathrm{d}\ell}{\mathrm{d}E_j/\mathrm{d}\ell} = \frac{\beta}{\sin\,\beta} \tag{73}$$

which means that as $\nu \to 0$ ($\beta \to 0$) it approaches unity and as $\ell \to \infty$ it goes to $\frac{w\ell}{4\lambda_j^2} = \frac{\nu}{4}$, which is the trend in figure 6(d).

5. Conclusions

In this paper, we have discussed the problem of laterally coupled long Josephson junctions in the form of a planar superlattice of alternating passive and active regions. We derived a set of equations for the phases in the windows. We considered a physically reasonable excitation pattern, with all the phases in the windows equal, which leads to coherent motion when dynamics is considered. In this specific case we obtained an analytic solution, which agrees very well with the numerical solution. It turns out that the nonlocality of the problem, which comes in through the coupling with the idle regions, is significant. For small nonlocality parameter ν ($\nu \ll 1$) the equation has the well-known fluxon solution except that its width is modified with respect to the usual sine-Gordon case. Namely, it becomes $w_f = \lambda_J\sqrt{\ell/w}$, which is similar to that found in [16] for small idle region widths, for a single window junction with lateral idle region.

Subsequently, we have calculated analytically various quantities, such as the fluxon content, N_x and N_z, the magnetic field components H_x and H_z, the Josephson current through a single window $j_n(z)$ and the energy densities $\mathcal{E}(x)$ and $\mathcal{E}(z)$. For $j_n(z)$, H_x and H_z we gave separate formulae in two limiting cases, for small and large nonlocality parameters.

For the specific analytical solution we have described, the fluxon content N_z is zero, while $N_x = N$ fluxons, where N is the number of windows we consider. We also assume that the junction is long enough so that the fluxons do not feel the boundaries. The magnetic field rotates between windows, while at the same time it moves along windows. In the case of small nonlocality parameter, we recover the usual behaviour of the magnetic field in a single Josephson junction. The magnetic field components decay with increasing z in very different ways for small and large nonlocality parameters. They decay exponentially as $z \to \pm\infty$ in the former case, while they decay algebraically in the latter. This is also valid for the Josephson current density $j_n(z)$.

The energy density per unit length of the idle region $\mathcal{E}(x)$, and the energy density per unit junction length $\mathcal{E}(z)$, can be analysed in two parts, a magnetic part and a Josephson part. When $\nu \to 0$ (local limit), the integrated magnetic part equals the integrated Josephson part, as it should. For larger ℓ, part of the magnetic energy is stored in the idle region, depending on the nonlocality of the system. The integrated magnetic and Josephson energies increase smoothly with increasing idle region width, ℓ.

Acknowledgments

YuBG would like to express his thanks for the hospitality of the University of Crete, where part of this work was done. Part of this work was supported by a PENED grant.

Appendix A

In this section, we derive the set of equations (6)–(9). Using the Fourier transform with respect to z and t

$$\bar{\phi}(x,k,\omega) = \frac{1}{(2\pi)^2}\int_{-\infty}^{\infty} \mathrm{d}z \int_{-\infty}^{\infty} \mathrm{d}t\, \phi(x,z,t)\, \mathrm{e}^{-\mathrm{i}(kz-\omega t)} \tag{74}$$

one can represent equation (3) in the idle regions

$$\ell n + \frac{w}{2} < x < \ell(n+1) - \frac{w}{2} \qquad n = 0, \pm 1, \pm 2, \ldots \tag{75}$$

in the form

$$-\left(k^2 - \frac{\omega^2}{v_i^2}\right)\bar{\phi}(x,k,\omega) + \partial_x^2\bar{\phi}(x,k,\omega) = 0. \tag{76}$$

In the windows

$$|x - \ell n| < \frac{w}{2} \qquad n = 0, \pm 1, \pm 2, \ldots \tag{77}$$

the corresponding equation is

$$-\left(k^2 - \frac{\omega^2}{v_j^2}\right)\bar{\phi}(x,k,\omega) + \partial_x^2\bar{\phi}(x,k,\omega) = \frac{1}{\lambda_j^2}\overline{\sin\phi}. \tag{78}$$

The solution of equation (76) in the interval (75) has the form

$$\bar{\phi}(x,k,\omega) = A_n(k,\omega)\,\mathrm{e}^{-\kappa x} + B_n(k,\omega)\,\mathrm{e}^{\kappa x} \tag{79}$$

where

$$\kappa = \sqrt{k^2 - \frac{\omega^2}{v_i^2}}. \tag{80}$$

The condition that the phase ϕ and its derivative $\partial_x\phi$ be continuous at the interfaces between windows and idle regions leads to the relations

$$A_n\,\mathrm{e}^{-\kappa(\ell n + \frac{w}{2})} + B_n\,\mathrm{e}^{\kappa(\ell n + \frac{w}{2})} = \bar{\phi}\left(\ell n + \frac{w}{2}, k, \omega\right) \tag{81}$$

$$A_n\,\mathrm{e}^{-\kappa(\ell n + \frac{w}{2})} - B_n\,\mathrm{e}^{\kappa(\ell n + \frac{w}{2})} = -\frac{1}{\kappa}\partial_x\bar{\phi}(x,k,\omega)|_{x=\ell n+\frac{w}{2}} \tag{82}$$

where $\bar{\phi}(x,k,\omega)$ is the solution of the window equation (78). Let us integrate equation (78) with respect to x over the nth window. As a result, we get

$$\partial_x\bar{\phi}(x,k,\omega)|_{x=\ell n+\frac{w}{2}} - \partial_x\bar{\phi}(x,k,\omega)|_{x=\ell n-\frac{w}{2}} - w\left(k^2 - \frac{\omega^2}{v_j^2}\right)\bar{\phi}_n(k,\omega)$$
$$= \frac{1}{\lambda_j^2}\int_{\ell n-\frac{w}{2}}^{\ell n+\frac{w}{2}} \mathrm{d}x\,\overline{\sin\phi} \tag{83}$$

where we assumed that $\bar{\phi}_n(k,\omega)$ is almost constant within the small width w and used the abbreviation

$$\frac{1}{w}\int_{\ell n-\frac{w}{2}}^{\ell n+\frac{w}{2}} \mathrm{d}x\,\bar{\phi}(x,k,\omega) = \bar{\phi}_n(k,\omega). \tag{84}$$

Taking into account the boundary conditions given by equations (81) and (82) we can represent equation (83) for $\ell \gg w$ in the form

$$\frac{\kappa}{\sinh(\kappa\ell)}\left[\bar{\phi}\left((n+1)\ell - \frac{w}{2}, k, \omega\right) + \bar{\phi}\left((n-1)\ell + \frac{w}{2}, k, \omega\right)\right]$$
$$- \frac{\kappa}{\tanh(\kappa\ell)}\left[\bar{\phi}\left(n\ell + \frac{w}{2}, k, \omega\right) + \bar{\phi}\left(n\ell - \frac{w}{2}, k, \omega\right)\right] - w\left(k^2 - \frac{\omega^2}{v_j^2}\right)\bar{\phi}_n(k,\omega)$$
$$= \frac{1}{\lambda_j^2}\int_{\ell n-\frac{w}{2}}^{\ell n+\frac{w}{2}} \mathrm{d}x\,\overline{\sin\phi}. \tag{85}$$

Assuming the window width w to be thin compared with the Josephson length λ_j, we consider equation (85) in the limit $w \to 0$ under the conditions

$$\frac{w}{v_j^2} \equiv \frac{\lambda_1 + \lambda_2}{c^2}\frac{w}{\epsilon d_j} = \text{constant} \tag{86}$$

$$\frac{w}{\lambda_j^2} \equiv \frac{2e\mu_0(\lambda_1+\lambda_2)}{\hbar} J_c w = \text{ constant.} \tag{87}$$

These conditions mean that the window capacitance per unit length $\left(\sim\frac{w}{d_j}\right)$ and the critical Josephson current per unit length ($\sim J_c w$) are supposed to be kept constant when the width of the window decreases. The other term proportional to w is omitted. This approximation is well satisfied for wide fluxons.

Taking into account (see e.g. [15]) that in the small width limit the right-hand side of equation (85) can be approximated as

$$\frac{1}{w}\int_{\ell n-\frac{w}{2}}^{\ell n+\frac{w}{2}} \mathrm{d}x\, \overline{\sin\phi} \simeq \overline{\sin\phi_n} \tag{88}$$

where the function $\bar{\phi}_n$ is given by equation (84), we obtain that the dynamics of the superlattice of narrow Josephson junctions is governed by the set of equations

$$\frac{\kappa}{\sinh(\kappa\ell)}[\bar{\phi}_{n+1}(k,\omega)+\bar{\phi}_{n-1}(k,\omega)] - \frac{2\kappa}{\tanh(\kappa\ell)}\bar{\phi}_n(k,\omega) + w\frac{\omega^2}{v_j^2}\bar{\phi}_n(k,\omega) = \frac{w}{\lambda_j^2}\overline{\sin\phi_n}(k,\omega) \tag{89}$$

where $n = 0, \pm1, \pm2, \ldots$. Using the inverse Fourier transform we can represent equations (89) in real space and time variables as follows:

$$\frac{\hat{\kappa}}{\sinh(\hat{\kappa}\ell)}[\phi_{n+1}(z,t)+\phi_{n-1}(z,t)] - \frac{2\hat{\kappa}}{\tanh(\hat{\kappa}\ell)}\phi_n(z,t) - \frac{w}{v_j^2}\partial_t^2\phi_n(z,t) = \frac{w}{\lambda_j^2}\sin\phi_n(z,t) \tag{90}$$

where $n = 0, \pm1, \pm2, \ldots$, and $\hat{\kappa} \equiv \sqrt{-\partial_z^2 + \frac{1}{v_i^2}\partial_t^2}$ is the pseudo-differential operator defined as

$$\overline{\hat{\kappa}\phi}(k,\omega) \equiv \frac{1}{(2\pi)^2}\int_{-\infty}^{\infty}\mathrm{d}z\int_{-\infty}^{\infty}\mathrm{d}t\,\mathrm{e}^{-\mathrm{i}(kz-\omega t)}\sqrt{-\partial_z^2+\frac{1}{v_i^2}\partial_t^2}\phi(z,t) = \sqrt{k^2-\frac{\omega^2}{v_i^2}}\overline{\phi}(k,\omega). \tag{91}$$

It is worth noting that the set of equations (90) corresponds to the model of a superlattice of infinitely narrow Josephson junctions which is described by the equation

$$\left(\partial_x^2+\partial_z^2-\frac{1}{v_i^2}\partial_t^2\right)\phi = f(x)\left(\frac{1}{\lambda_j^2}\sin\phi+\frac{1}{v_j^2}\partial_t^2\phi\right) \tag{92}$$

with

$$f(x) = w\sum_n \delta(x-x_n) \qquad x_n = n\ell \quad n = 0, \pm1, \pm2, \ldots. \tag{93}$$

Appendix B

The nonlocal character of the window junction dynamics is clearly seen if we consider, for example, the second term on the lhs of equation (14). Taking into account the well-known expansion in series of simple fractions [17] and definition (15) of the operator $\hat{\kappa}$, we can write

$$\begin{aligned}\frac{\hat{\kappa}\ell}{\tanh\ell\hat{\kappa}}\phi_n(z,t) &= \phi_n(z,t) + 2\ell^2\sum_{m=1}^{\infty}\frac{1}{\hat{\kappa}^2\ell^2+m^2\pi^2}\hat{\kappa}^2\phi_n(z,t)\\ &= \phi_n(z,t) - \int_{-\infty}^{\infty}\mathrm{d}z'\int_{-\infty}^{t}\mathrm{d}t'\,\mathcal{K}(\zeta)\theta(\zeta)\left(\partial_{z'}^2-\frac{1}{v_i^2}\partial_{t'}^2\right)\phi_n(z',t').\end{aligned} \tag{94}$$

Here $\theta(\zeta)$ is the step function and the abbreviation $\zeta = \sqrt{v_i^2(t-t')^2 - (z-z'x)^2}$ was used. The kernel $\mathcal{K}(\zeta)$ is given by the expression

$$\mathcal{K}(\zeta) = 2\frac{1}{(2\pi)^2}\int_{-\infty}^{\infty} \mathrm{d}k \int_{-\infty}^{\infty} \mathrm{d}\omega\, \mathrm{e}^{\mathrm{i}(k(z-z')-\omega(t-t'))} \sum_{m=1}^{\infty} \left(k^2 - \frac{\omega^2}{v_i^2} + \frac{m^2\pi^2}{\ell^2}\right)^{-1}$$

$$= v_i \sum_{m=1}^{\infty} J_0\left(\frac{m\pi}{\ell}\zeta\right) = -\frac{1}{2} + \frac{\ell}{\pi\zeta} + \frac{2\ell}{\pi}\sum_{m=1}^{N} \frac{1}{\sqrt{\zeta^2 - 4m^2\ell^2}} \tag{95}$$

for $2N\ell < \zeta < 2(N+1)\ell$, where $N = 0, 1, 2, \ldots$, is a natural number and $J_0(x)$ is the Bessel function. We see from equation (95) that when $\zeta < 2\ell$ $(N = 0)$ the kernel $\mathcal{K}(\zeta)$ has the form

$$\mathcal{K}(\zeta) = -\frac{1}{2} + \frac{\ell}{\pi\sqrt{v_i^2(t-t')^2 - (z-z')^2}} \tag{96}$$

which corresponds to the signal motion along the junction only. But when $2\ell < \zeta < 4\ell (N = 1)$

$$\mathcal{K}(\zeta) = -\frac{1}{2} + \frac{\ell}{\pi\sqrt{v_i^2(t-t')^2 - (z-z')^2}} + \frac{2\ell}{\pi\sqrt{v_i^2(t-t')^2 - (z-z')^2 - 4\ell^2}} \tag{97}$$

and the last term in this expression describes the motion of the signal inside the idle region and its reflection from the neighbour windows. It is seen from equation (95) that increasing ζ makes the pathways with 3, 5, 7, ... possible, and so on, reflections from the neighbour windows. Note that the kernel which arises in the first term on the lhs of equation (14) has a structure similar to equation (95) but the number of reflections here is always even which is quite natural: this term in equation (14) describes the coupling between windows and depends on the phases of the neighbouring junctions.

References

[1] Bi B, Han S and Lukens J E 1993 *Appl. Phys. Lett.* **62** 2745
[2] Benz S P and Burroughs C J 1991 *Appl. Phys. Lett.* **58** 2162
[3] Booi P A A and Benz S P 1994 *Appl. Phys. Lett.* **64** 2163
[4] Petraglia A, Ustinov A V, Pedersen N F and Sakai S 1995 *J. Appl. Phys.* **77** 1171
[5] Monaco R, Polcari A and Capogna L 1995 *J. Appl. Phys.* **78** 3278
[6] Ustinov A V, Kohlstedt H and Heiden C 1994 *Appl. Phys. Lett.* **65** 1457
[7] Holst T, Bindslev Hansen J, Groenbech-Jensen N and Blackburn J A 1990 *Phys. Rev.* B **42** 127
[8] Carapella G, Costabile G and Sabatino P 1998 *Phys. Rev.* B **58** 15094
[9] Flytzanis N, Lazarides N, Chiginev A, Kurin V and Caputo J G 2000 *J. Appl. Phys.* **88** 4201
[10] Mittra R (ed) 1973 *Computer Techniques for Electromagnetics (International Series of Monographs in Electrical Engineering vol 7)* (Oxford: Pergamon)
[11] Barone A and Paterno G 1982 *Physics and Applications of the Josephson Effect* (New York: Wiley)
[12] Matsuno Y 1995 *Int. J. Mod. Phys.* B **9** 1985
[13] Alfimov G I and Popkov A F 1995 *Phys. Rev.* B **52** 4503
[14] Joseph R I 1977 *J. Phys. A: Math. Gen.* **10** L225
[15] Caputo J G, Flytzanis N, Gaididei Yu and Vavalis E 1996 *Phys. Rev.* E **54** 2092
[16] Caputo J G, Flytzanis N and Vavalis E 1996 *Int. J. Mod. Phys.* C **7** 191
[17] Gradsteyn I S and Ryzhik I M 1965 *Table of Integrals, Series, and Products* (New York: Academic)
[18] Caputo J G, Flytzanis N, Kurin V, Lazarides N and Vavalis E 1999 *J. Appl. Phys.* **85** 7282